Supplementary Information
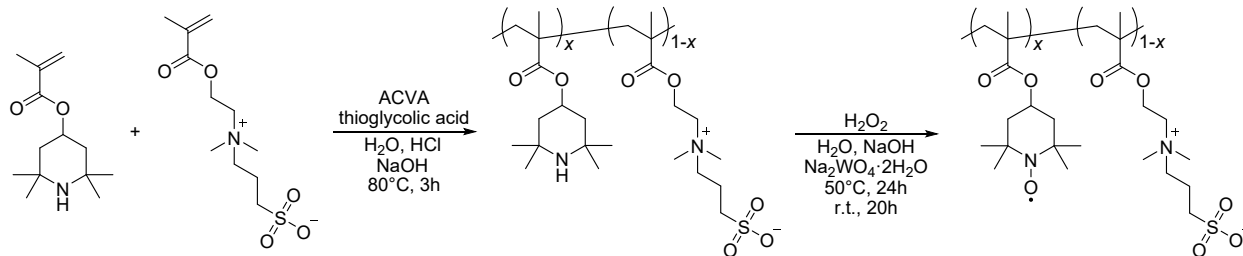
Charge-transport kinetics of dissolved redox-active polymers for rational design of flow batteries
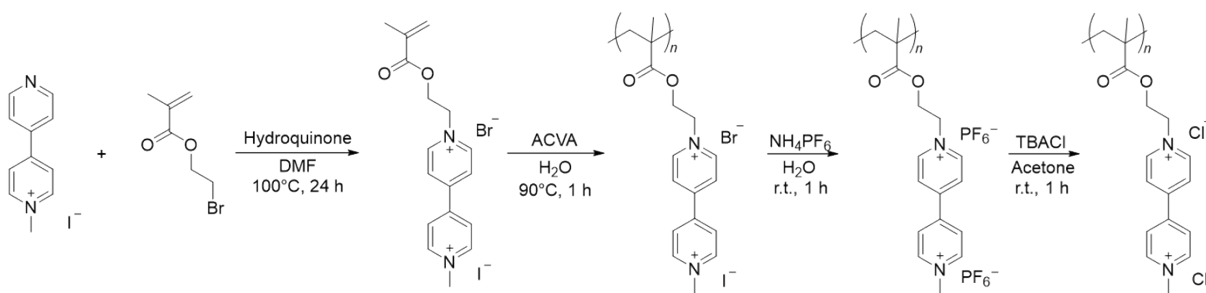
Kan Hatakeyama-Sato,* Yuto Igarashi, Kenichi Oyaizu*

Department of Applied Chemistry, Waseda University, 3-4-1 Okubo, Shinjuku, Tokyo 169-8555,

Japan

Scheme S1. Synthesis of P(TMA-*r*-SBMA). ACVA: 4,4'-azobis(4-cyanovaleric acid):

Scheme S2. Synthesis of PVMA. TBACl: tetrabutylammonium Chloride.

Supplementary discussions

Contribution of electron hopping to flux

Apparent charge flux consists of physical diffusion and electron hopping (**Eq 2**). In most cases, the electron hopping flux (J_{et}) is negligible compared to physical diffusion (J_{phys}), yielding $J_{app} \cong J_{phys}$ (or $J_{phys} \gg J_{et}$) or **Eq 1** ($D_{app} = D_{phys}$).[1-4] Here, we validate the approximation.

The precise estimation of J_{et} is usually inaccessible because of the uncertainty of the concentration gradient of the local redox sites (∇C_{local}).[5] However, we can assume $J_{app} \cong J_{phys}$ considering the experimental relation of D_{phys} and D_{et}. According to a Dahms-Ruff model, D_{et} is a function of the electron self-exchange reaction rate constant $k_{ex,app}$ (**Eq 1**).[6, 7] The hopping distance δ is often approximated as $(N_A C_{bulk})^{-1/3}$ (N_A: Avogadro constant). Thus, the diffusion coefficient D_{et} will be at most 2×10^{-7} cm^2/s under the conditions of large $k_{ex,app} = 10^8$ M^{-1}s^{-1} of small molecules[7] and a standard flow cell concentration of $C_{bulk} = 1$ M.

On the other hand, D_{et}, the physical diffusion coefficient of molecules is estimated by the Stokes-Einstein equation (**Eq 5**). The coefficient D_{phys} becomes around 5×10^{-6} cm^2/s for a typical radius of $r = 0.5$ nm and $\eta = 0.89$ mPa·s of water at room temperature. The value is much larger than $D_{et} = 2 \times 10^{-7}$ cm^2/s.

The molecular radius will be larger with macromolecular systems,[2] leading to the smaller D_{phys} of 1×10^{-7} cm^2/s at $r = 20$ nm. At the same time, $k_{ex,app}$ of macromolecules becomes smaller due to the restricted motions of redox moieties attached to polymer backbones.[7] If $k_{ex,app}$ is 1/10 smaller[7] than the small species, D_{et} will be 2×10^{-8} cm^2/s.

Therefore, the experimental relationship of $D_{phys} \gg D_{et}$ (or at least $D_{phys} > D_{et}$) and the approximation of $D_{app} = D_{phys}$ could be valid for various redox systems in low viscous solutions. The relation yields **Eq 1** ($D_{app} = D_{phys}$), indicating that physical diffusion of redox molecules is critical with most redox-flow systems, except for special cases such as nanoparticles giving small $D_{phys} \cong 10^{-9}$ cm^2/s.[5]

Although the absolute contribution of electron hopping is less significant than physical diffusion, their molecular processes could be of scientific interest. For polymer systems, the hopping consists of intra- and inter-chain charge transfer. Intra-chain hopping becomes more dominant than inter-chain hopping under basic measurement conditions of D_{app}, where polymers are diluted.[3] In this case, the concentration should be below the overlapping value, where the macromolecules contact each other (e.g., around 50 mM for polystyrene with $M_w = 1.4 \times 10^6$; the criterion is a function of molecular weight).[8, 9] In practical flow cells, active materials are concentrated for energy density (> 0.1 M).[3] The polymer concentration will exceed the overlapping threshold,[8, 9] and inter-chain hopping will play more significant roles, whose quantitative evaluation is our ongoing study.

A simple diffusion assumption of electron hopping might not be appropriate at the molecular-chain level because electron self-exchange reactions proceed randomly among the redox units.[7] Cooperative diffusion of molecular chains and electrical charges should be considered for higher accuracy. The development of more detailed physical models, under the support of experimental results, is needed in the future.

Comparison of $\overline{r_n^{-1}}$ and $1/\overline{r}_n$ to determine the diffusion coefficient

Here, we briefly discuss the difference of $\overline{r_n^{-1}}$ and $1/\overline{r}_n$ for the estimation of $D_{phys,chain}$ (**Eq 6**). For simplicity, we consider two particles having radii of 10 and 1 of arbitrary units (**Figure 2e**). According to the Stokes-Einstein equation, their relative physical diffusion coefficients could be 10/10 = 1 and 10/1 = 10 for the larger and smaller particles, respectively. Their average coefficient becomes 5.5 (i.e., **Eq 6**). In contrast, if the average radius (DLS output) is used in the Stokes-Einstein equation, a wrong value of 10/(average radius) = 10/5.5 = 1.8 is obtained for diffusion coefficient estimation. Since the charge flux of redox reactions is proportional to $D_{phys,chain}$ according to Fick's law (**Eq 2**), a chargeable capacity of flow cells is dominated by the coefficient. The formal treatment of **Eq 6** is preferred for a more accurate discussion.

Estimation of electrode reaction rate constant by RDE

RDE is a popular method of determining D_{app} and k^0. On the other hand, attention is needed for the estimation of the latter value with large k_0 because the contribution of the reverse reaction is unavoidable.[10] Here, we briefly summarize the theory of RDE, focusing on parameter estimation errors.

For a simple one-step, one-electron, reversible redox system, the observed current density j during RDE is given by **Eq 9**.

	$$\frac{1}{j} = \frac{1}{F(k_f C_{Red} - k_b C_{ox})} + \frac{D_{Red}^{-2/3} k_f + D_{ox}^{-2/3} k_b}{0.62 F \upsilon^{-1/6} \omega^{1/2}(k_f C_{Red} - k_b C_{ox})}$$ $$k_f = k^0 \exp\left(\frac{(1-\beta)F}{RT}\eta\right)$$ $$k_b = k^0 \exp\left(\frac{(-\beta)F}{RT}\eta\right)$$	**Eq 9**

(C: concentration, D: diffusion coefficient, υ: kinetic viscosity, ω: rotation rate, β: symmetry coefficient, η: overpotential, Red: reduced species, and Ox: oxidized species)

When the absolute overpotential $|\eta|$ is sufficiently large, a conventional equation for Koutecký–Levich plot is obtained (**Eq 10**).

	$$\frac{1}{j} = \frac{1}{F k_f C_{Red}} + \frac{1}{0.62 F D_{Red}^{2/3} \upsilon^{-1/6} \omega^{1/2} C_{Red}}$$ (for cathodic reaction)	**Eq 10**

The previous paper calls attention to the assumption that ignoring the reverse reaction is not always correct, and it will induce estimation errors (about 200% estimation error of current density in maximum).[10]

The slope of Koutecký–Levich plots can also change by the contribution of backward reaction. For a simple system of $D_{Red} = D_{Ox}$, the slope term in **Eq 9** becomes **Eq 11**.

$$(slope) = \frac{D_{Red}^{-2/3}k_f + D_{ox}^{-2/3}k_b}{0.62Fv^{-1/6}(k_f C_{Red} - k_b C_{ox})} = \frac{D_{Red}^{-2/3}}{0.62Fv^{-1/6}}\left(\frac{\exp\left(\frac{(1-\beta)F}{RT}\eta\right) + \exp\left(}{\exp\left(\frac{(1-\beta)F}{RT}\eta\right)C_{Red} - \exp\left(}\right) \qquad \textbf{Eq 11}$$

The dependence of slope on η was plotted under an arbitrary unit satisfying $\frac{D_{Red}^{-2/3}}{0.62Fv^{-1/6}} = 1, \beta = 0.5, C_{Red} = 0.999, C_{Ox} = 0.001$, and $T = 298\,K$ (**Figure S5**). The calculated slope almost converged at $\eta > 100$ mV, which corresponded to the assumption of negligible backward reaction. On the other hand, the slope increased to around 2 with smaller overpotentials. The unfavorable increase also indicated that the backward reaction was unavoidable even with the intercept term in **Eq 9**.

Experimentally, many RDE data exhibited non-parallel Koutecký–Levich plots because of the small applied overpotentials (< 100 mV) and non-negligible effects of backward reactions(**Figure S4**, **Figure S6**, **Figure S7**). Analysis with large $|\eta|$ was difficult because the experimental currents quickly saturated to the limited currents (i.e., plateaus) because of the large k^0. This is an intrinsic limitation of the Koutecký–Levich analysis to evaluate the rate constant.[10]

Although RDE is not an optimal method to estimate k^0 with large values, the convenient technique is often employed.[10] The estimation did not drastically differ from values measured by other techniques.[11]

Diffusion model of permeation

The diffusion coefficient for the permeation of active materials through a separator, D_{perm}, was estimated according to Fick's law. We consider two cells separated by a self-standing film with a thickness of d (**Figure S11**). In the cells, liquids are filled with a volume of V. The left (or right) liquid contained a target material with a concentration of C_1 (or C_2). There should be no concentration gradient in bulk (i.e., sufficient stirring is assumed).

The flux of the target compound to the opposite side can be estimated by a standard boundary film model of chemical engineering. Overall mass transfer coefficient K consists of film mass transfer coefficients k_1 and k_2, and the coefficient for the separator k_d (**Eq 12**).

$$\frac{1}{K} = \frac{1}{k_1} + \frac{1}{k_d} + \frac{1}{k_2}$$ **Eq 12**

We should assume that the diffusion of active materials in the separator must be much smaller than the mass transfer via boundary films of liquids ($k_d \ll k_1, k_2$). In that case, the overall mass transport will be dominated by the permeation through the polymer film (**Eq 13**).

$$K \cong k_d$$ **Eq 13**

In the separator, the concentration gradient of active materials can be constant ($\frac{dC}{dx} = const.$, where x is the position in the axis). The linear approximation comes from the assumption that the concentration relaxation in the separator occurs much faster than the time-dependent changes of C_1 and C_2 (i.e., slow permeation). The overall equation practically matches Fick's 1st law for the permeation flux J_{perm} (**Eq 14**)

$$J_{perm} = -K(C_2 - C_1)$$
$$= -k_d(C_2 - C_1)$$
$$= -\frac{1}{d}D_{perm}(C_2 - C_1)$$
$$= -D_{perm}\frac{\Delta C}{d}$$
$$(\Delta C = (C_2 - C_1))$$

Eq 14

The time-dependent change of C_1 can be derived from **Eq 14**, using the flux area A (**Eq 15**)

A

$$V\frac{dC_1}{dt} = -AJ_{perm}$$
$$\therefore \frac{Vd}{DA}\frac{dC_1}{dt} = -2C_1 + C_0$$
$$(C_1 + C_2 = C_0 \ (const.))$$

Eq 15

Integrating the differential equation with $C_1 = C_0$ and $C_2 = 0$ at $t = 0$ yields **Eq 16**.

$$\ln(2C_1 - C_0) = -\frac{2D_{perm}A}{d}\frac{}{V}t + \ln C_0$$

Eq 16

Evaluating diffusion coefficient for permeation

Linear fitting of $\ln(2C_1 - C_0)$ against time yielded the diffusion coefficient for the permeation of active materials (**Figure S12**). The experimental trends of TEMPOL and ethylviologen were almost linear, indicating that the proposed diffusion model was valid. The estimated diffusion coefficients were 3×10^{-8} and 7×10^{-11} cm^2/s for TEMPOL and ethylviologen, respectively.

In contrast to small molecules, nonlinear responses were detected with the logarithmic plot (**Figure S12**). After the concentration decreased in the early stages, it was saturated at $t > 20$ hr. The reason may be explained by the trace amount of oligomeric species that occurred during the synthesis of polymers. Linear fitting during the early stages yielded $D_{perm} = 9 \times 10^{-10}$ and 8×10^{-11} cm^2/s for P(TMA-*r*-SBMA) and PVMA, respectively. The values were comparable to TEMPOL and ethylviologen, indicating that oligomeric species induced the permeation. Technologically, carefully removing the tiny molecules by optimal purification is essential to avoid permeation.

The permeation of the polymer became much slower in the late stages. The coefficient became much smaller 6×10^{-12} cm^2/s for P(TMA-*r*-SBMA). The concentration of PVMA slightly increased over time, probably because of the limited detection accuracy of the redox species. According to the slope, D_{perm} should be less than 10^{-12} cm^2/s. The smaller coefficients show the benefit of polyelectrolyte design as active materials of flow batteries.

Estimation of battery performances from kinetic parameters

Electrochemical overpotential η can be estimated from the Butler-Volmer equation.[12]

	$$I = FAk^0(C_{ox}e^{-\alpha f\eta} - C_{red}e^{-(1-\alpha)f\eta})$$ $$f = zF/RT$$	**Eq 17**

(I: observed current, F: Farraday's constant, A: current collector area, C_{ox} (C_{red}): concentration of oxidized (reduced) species), α: charge-transfer coefficient, z: number of electrons involved in the reaction, R: gas constant, and T: temperature)

For instance, a current density will become around 0.18 mA/cm² for P(TMA-r-SBMA) with $\eta = 10$ mV under the condition of $k^0 = 0.0013$ cm/s, $\alpha = 0.5$, $T = 298$ K, $z = 1$, and $C_{ox} = C_{red} = 3.7$ mM (corresponding to the half-charged state of the 200 mAh/L catholyte).

Fick's law[12] derives the estimation of chargeable capacity. Initially, the concentration of active material is set to be C_{init} (**Figure S16a**). During chronopotentiometry, a constant current is made, whose flux J is given by $J = D_{app}\Delta C/\delta = I/zFA$), where ΔC is concentration decrease in a fluid film near the current collector and δ is the thickness of the fluid film. The most simple approximation for the system is to introduce only the liquid film and bulk concentration phase (**Figure S16b**). The concentration changes linearly in the boundary and is constant in other regions. Constant flux requires fixed ΔC and δ during the measurement (**Figure S16c**). Chronopotentiometry stops when the concentration of active material at the current collector becomes zero (**Figure S16d**). The chargeable part of concentration is given by $C_{init} - \Delta C$, which yields rechargeable capacity. Note that the simple assumption does not reflect the actual porous electrode systems with more complex concentration gradients. The approximation is valid only

when stirring or flowing is conducted intensely, like RDE. Electrochemical simulations would be needed for more precise calculations.[13, 14]

$$(\text{Obtainable capacity}) = C_{cap} \times (liquid\ volume)$$
$$C_{cap} = C_{init} - C_{fin}$$
$$= C_{init} - \frac{\delta I}{D_{app} F A}$$

Eq 18

(C_{cap}: (dis)chargeable capacity in concentration (mol/L), C_{init}: initial concentraion, C_{fin}: final bulk concentration after electrolysis, δ: thickness of the fluid film, I: applied current, F: Farraday's constant, and A: current collector area):

We detected no remarkable voltage loss in the charge/discharge curves, meaning that electrolyte and electrode resistances were small (**Figure 5d**). According to the Butler-Volmer equation, theoretical overpotential can be evaluated.[12] The estimated overvoltage to induce a current density of 0.2 mA/cm^2 for the catholyte was only 10 mV. The overvoltage will also become much smaller by using porous current collectors with larger surface areas. Thus, the practical current density[3] of > 1 mA/cm^2 is easy to be achieved by electrochemical reactions of polymers even though they display lower k^0 than small molecules (Table 1).[3]

Estimation of experimental capacity and rate performances from D_{app} is more challenging than overpotentials. Charge/discharge measurements regularly utilize constant current chronopotentiometry: it stops when the concentration of active material at the current collector becomes zero.[12] The theoretical chargeable capacity can be roughly estimated under an ideal

system where the concentration of a bulk phase is constant (i.e., corresponding to the cases where liquids are stirred or flowed sufficiently, **Figure S16**). The equation clarifies the significance of D_{app}, apparent fluid film thickness δ, and area of current collector A. The ratio of δ/A can be estimated from the experimental charging capacity and D_{app}. In the case of P(TMA-*r*-SBMA), a ratio of $A/\delta = 0.2$ cm^2 / 1 μm was obtained. The ratio indicates that an apparent electrode area of only 0.2 cm^2 was enough to charge the cell, having a virtual fluid film thickness of 1 μm on the current collector.

Since D_{app} tends to be smaller with polymers, a response rate could be an issue of cell design. From the derived equation, the ratio of A/δ has to be several orders larger than small molecules to charge cells in the same charging/discharging time. Bigger current collectors and faster flowing will solve the problem. Still, the issue may not be critical because flow cells do not mainly focus on response rates.[2]

Experimental estimation of δ and A is a challenge for a more rational design of flow cells. The surface area A can be evaluated by measuring the gas adsorption volume under dry conditions or electrochemical capacitance.[12] Application of fluid dynamics models could estimate δ.[12-14] More work will be needed to reveal the relationships between D_{app} and experimental capacities.
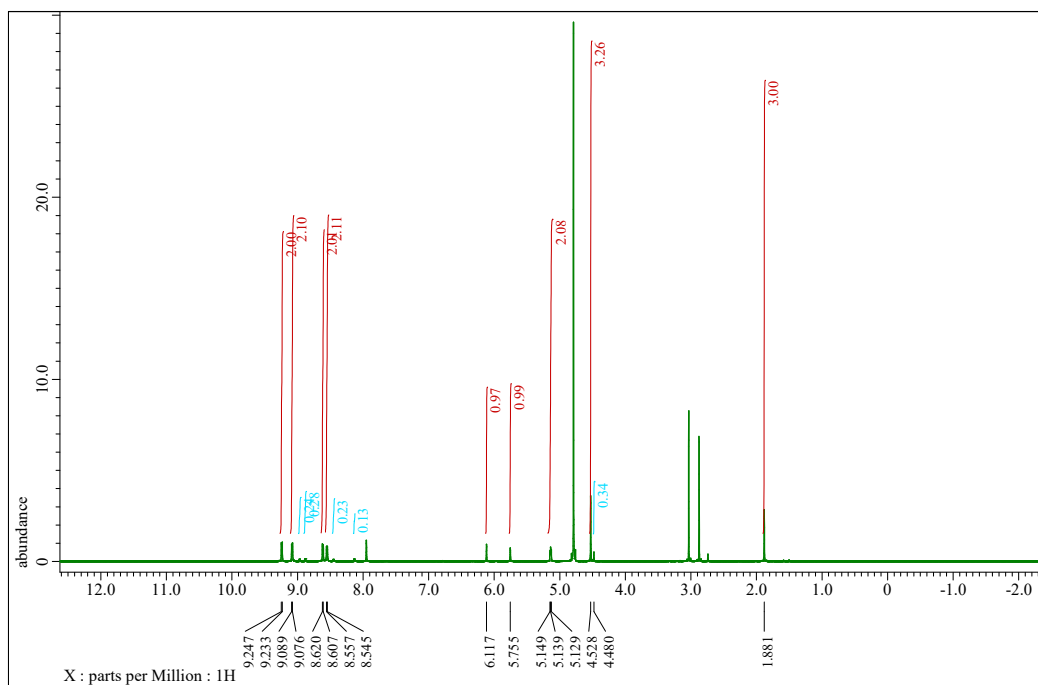
Figure S1. ^{1}H-NMR spectrum of the viologen monomer in D$_2$O.
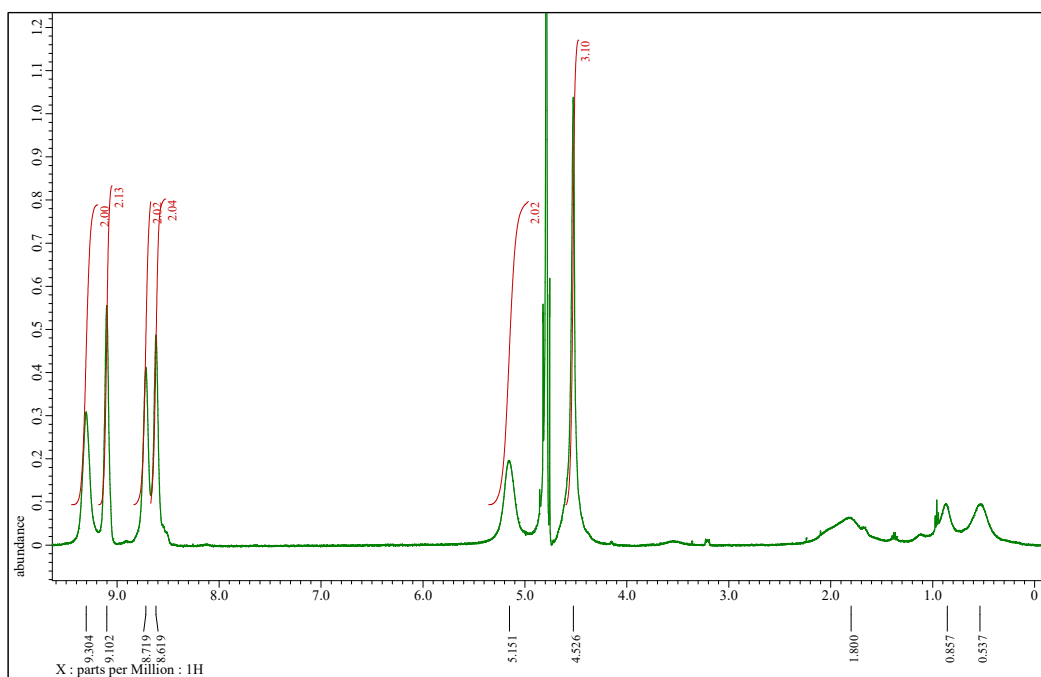
Figure S2. ^{1}H-NMR spectrum of PVMA in D$_2$O.
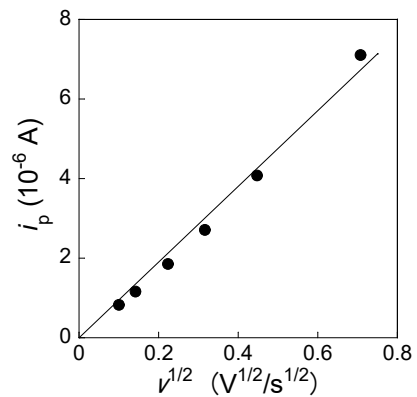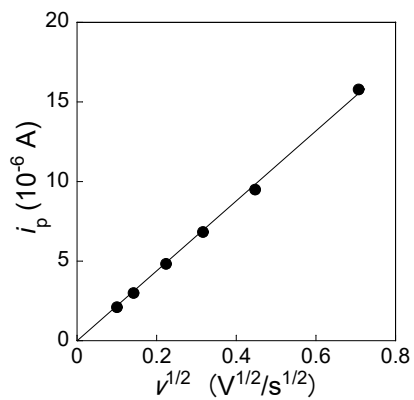
a)   b)

Figure S3. Peak current versus scan rate for a) cathode- and b) anode-active materials, shown in **Figure 3a** and **d**.
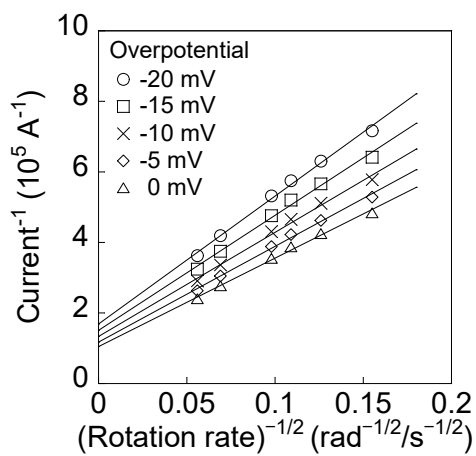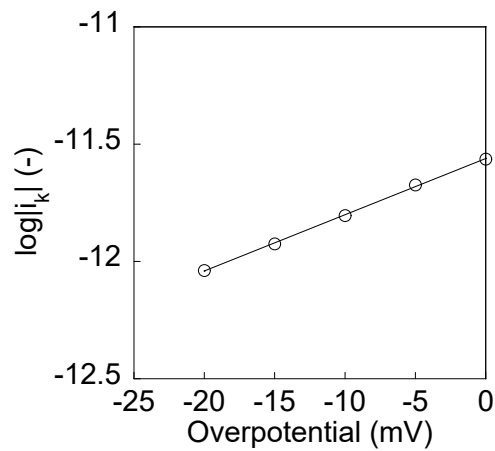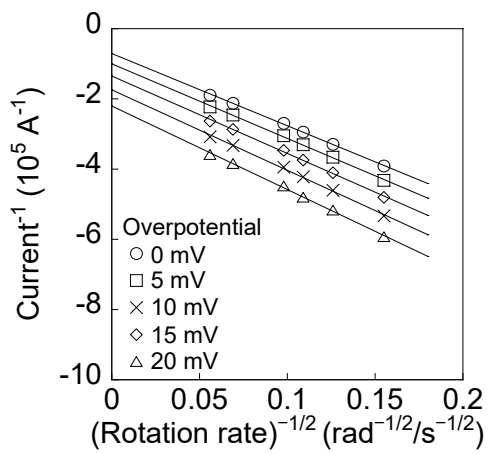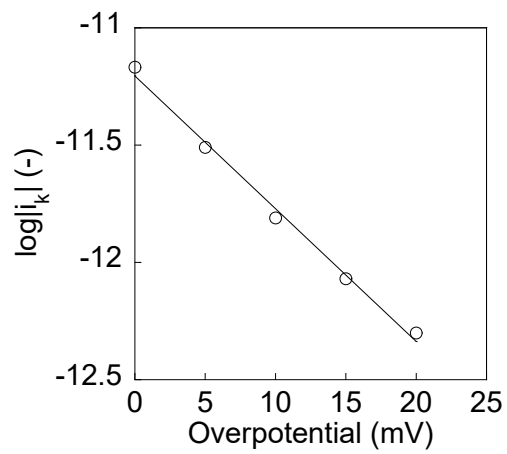
Figure S4. Tafel plots for a) cathode- and b) anode-active materials, obtained from RDE data of Figure 3**c** and **e.**
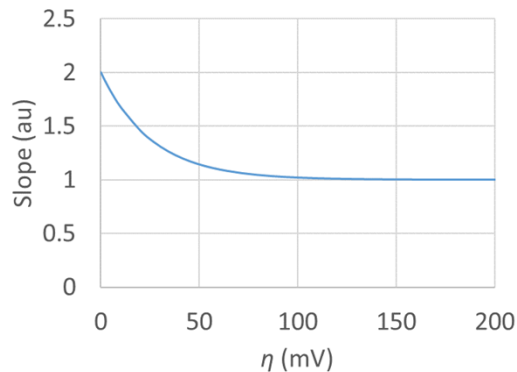
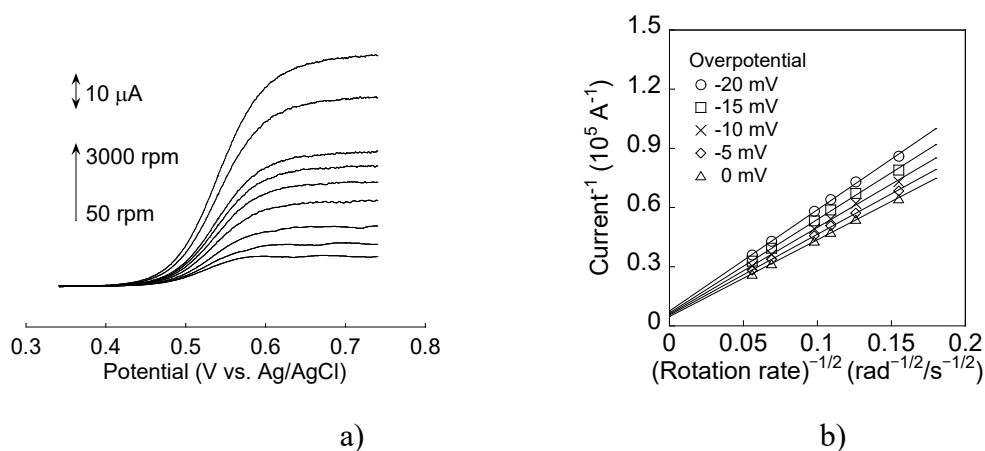**Figure S5.** The theoretical slope of Koutecky-Levich plot estimated from **Eq 11**.

a)

b)

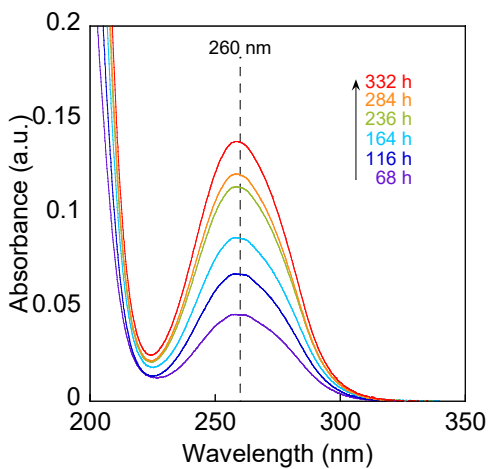**Figure S6.** a) Hydrodynamic voltammograms of 1 mM TEMPOL, scanned at 10 mV/s. and b) its Koutecky-Levich plot.

a)

b)
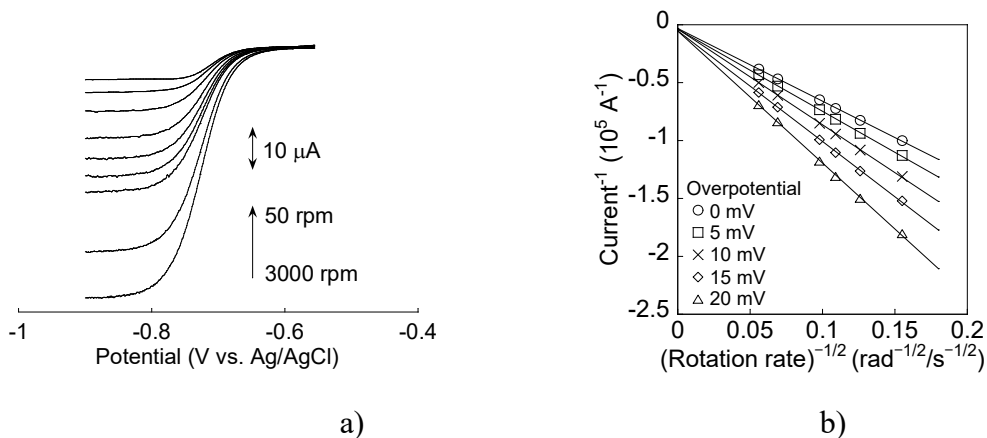
Figure S7. a) Hydrodynamic voltammograms of 1 mM ethylviologen, scanned at 10 mV/s. and b) its Koutecky-Levich plot.

C1

C2

C3

C4

C5

C6

C7
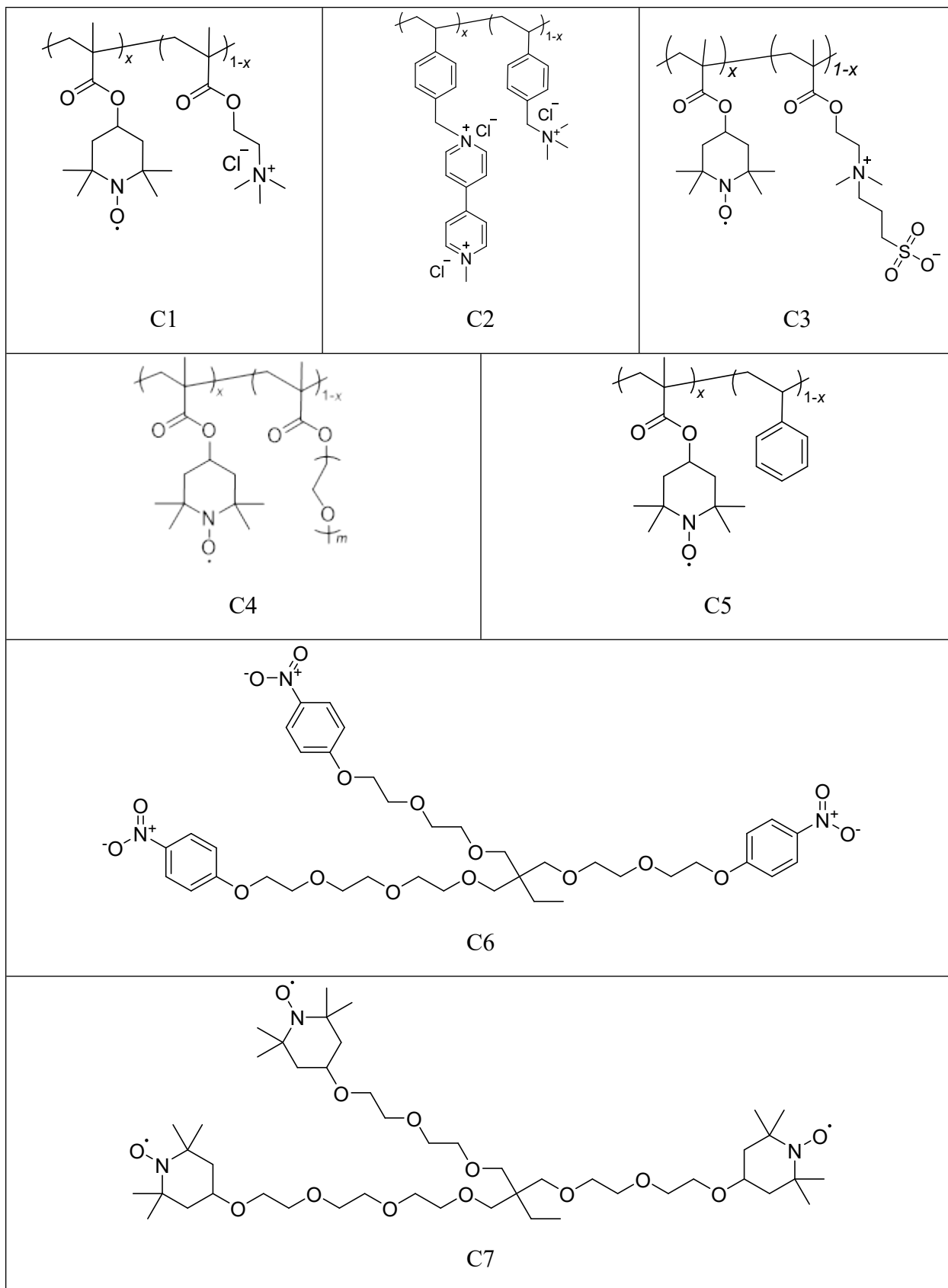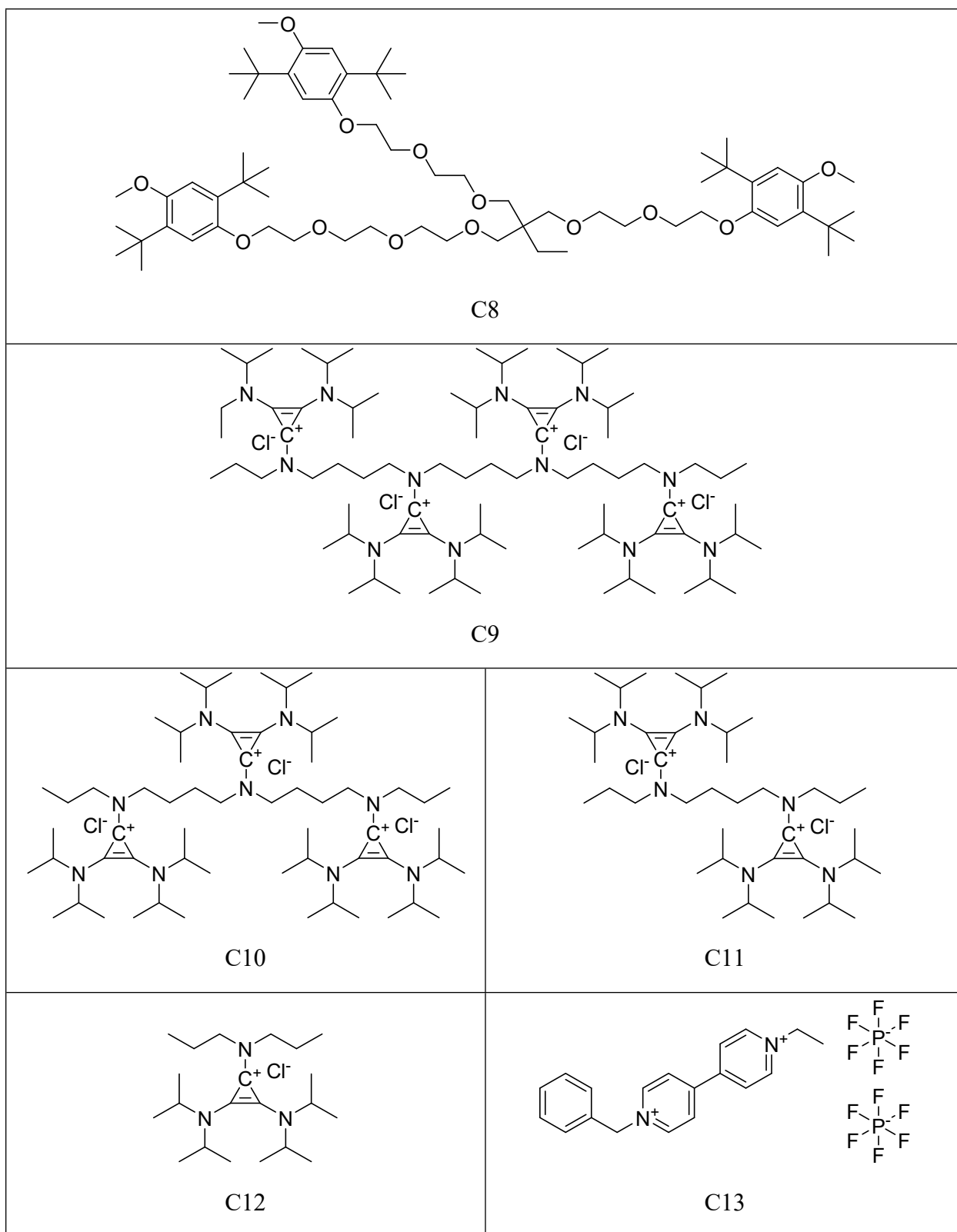
**Figure S8.** Chemical structures discussed in Table 1.

a)

b)

c)

d)

Figure S9. Nyquist plots for a) anion-exchange membrane (mainly used in this study), b) Nafion, and c) SELEMION. Blue texts show measurement frequencies. X-intercepts were regarded as membrane resistances. d) Comparison of the three impedance data with the normalized area (1.77 cm^2).
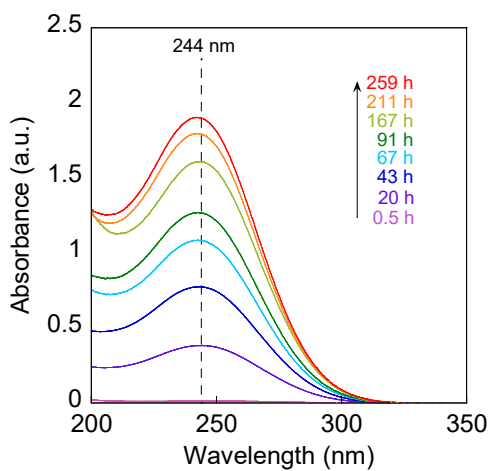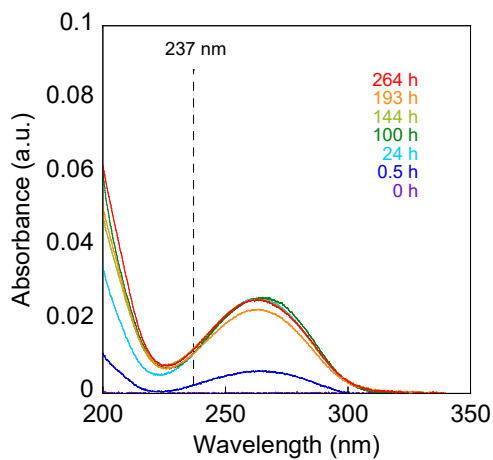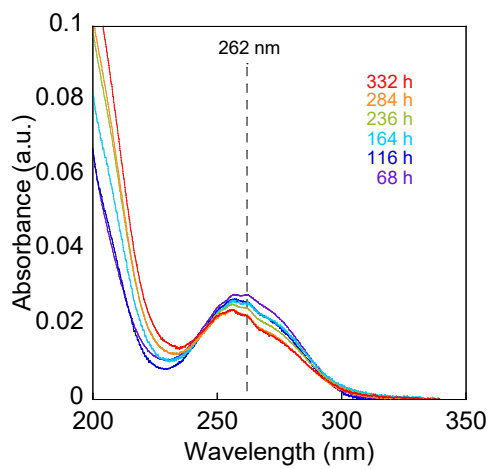
**Figure S10.** UV-vis spectra for the counter side of a) TEMPOL, b) P(TMA-*r*-SBMA), c) ethylviologen, and d) PVMA.
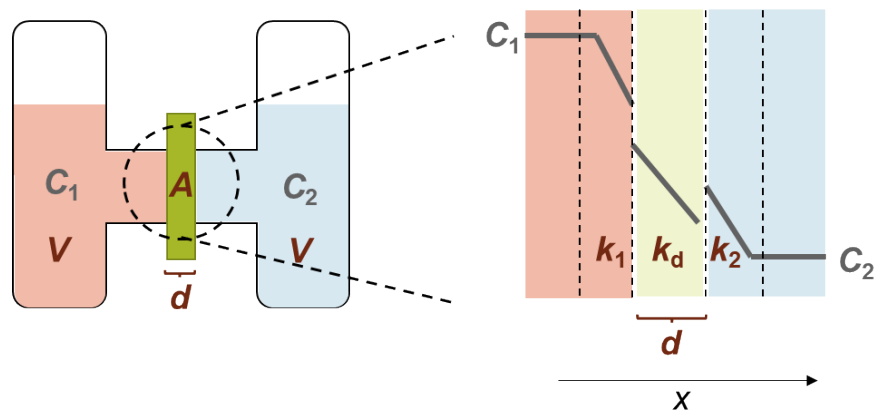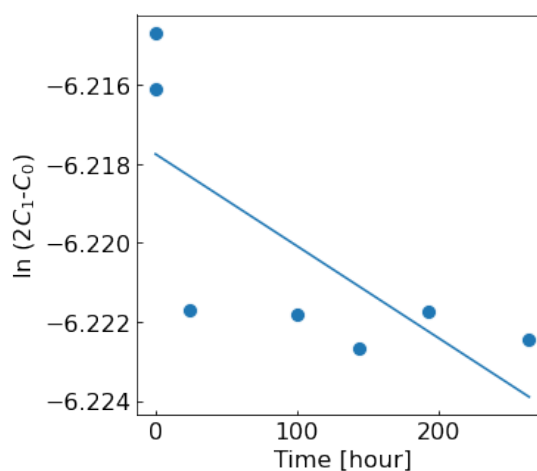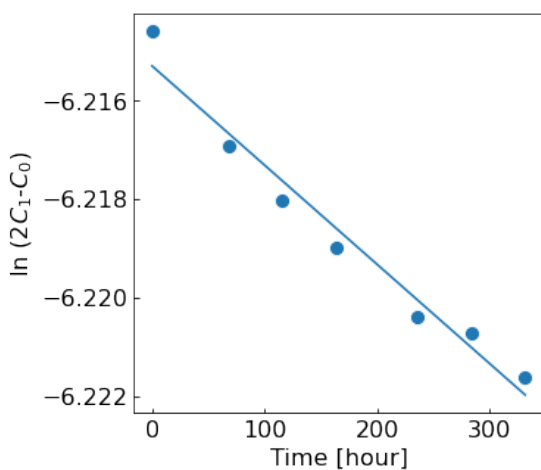
a)
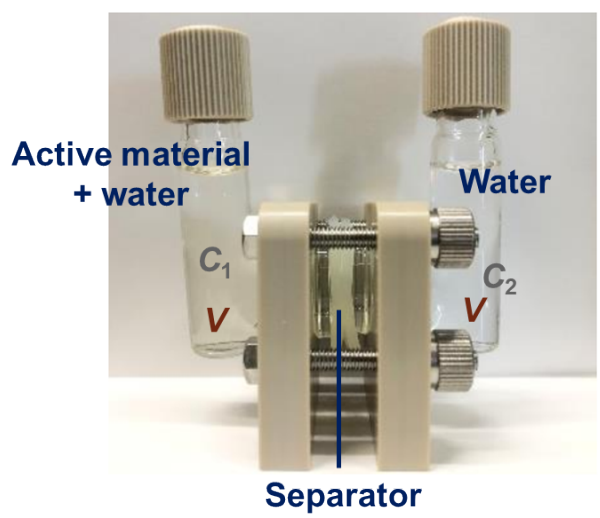
b)

Figure S11. Configuration of an H-type cell for permeation measurement with a) illustration and b) Photograph. In the actual tests, two vials were fixed using screws. In the center, an anion-exchange membrane was sandwiched with round-shaped rubber seals to avoid liquid leakage.
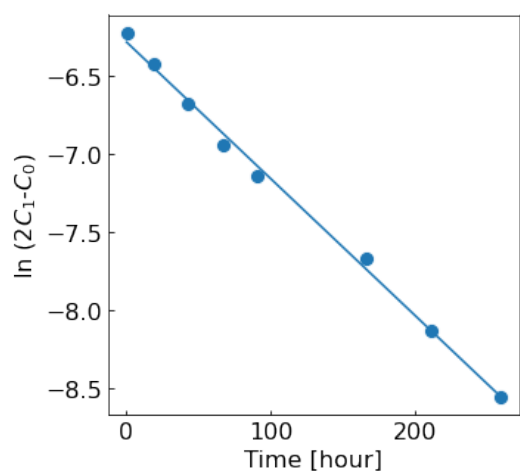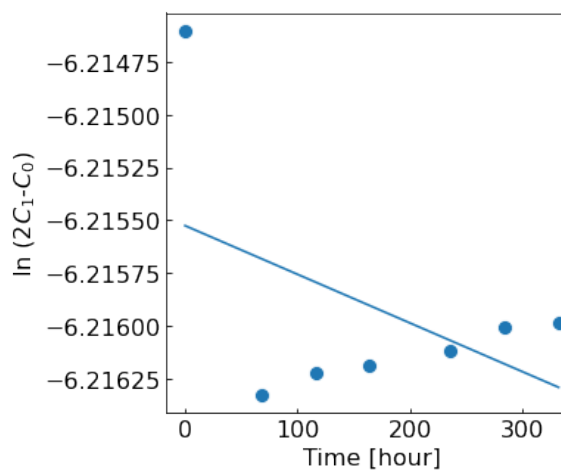
Figure S12. Diffusion coefficient analysis of a) TEMPOL, b) P(TMA-r-SBMA), c) ethylviologen, and d) PVMA. Original data were obtained as **Figure 5b,c**, and processed by a diffusion model described in the method section.
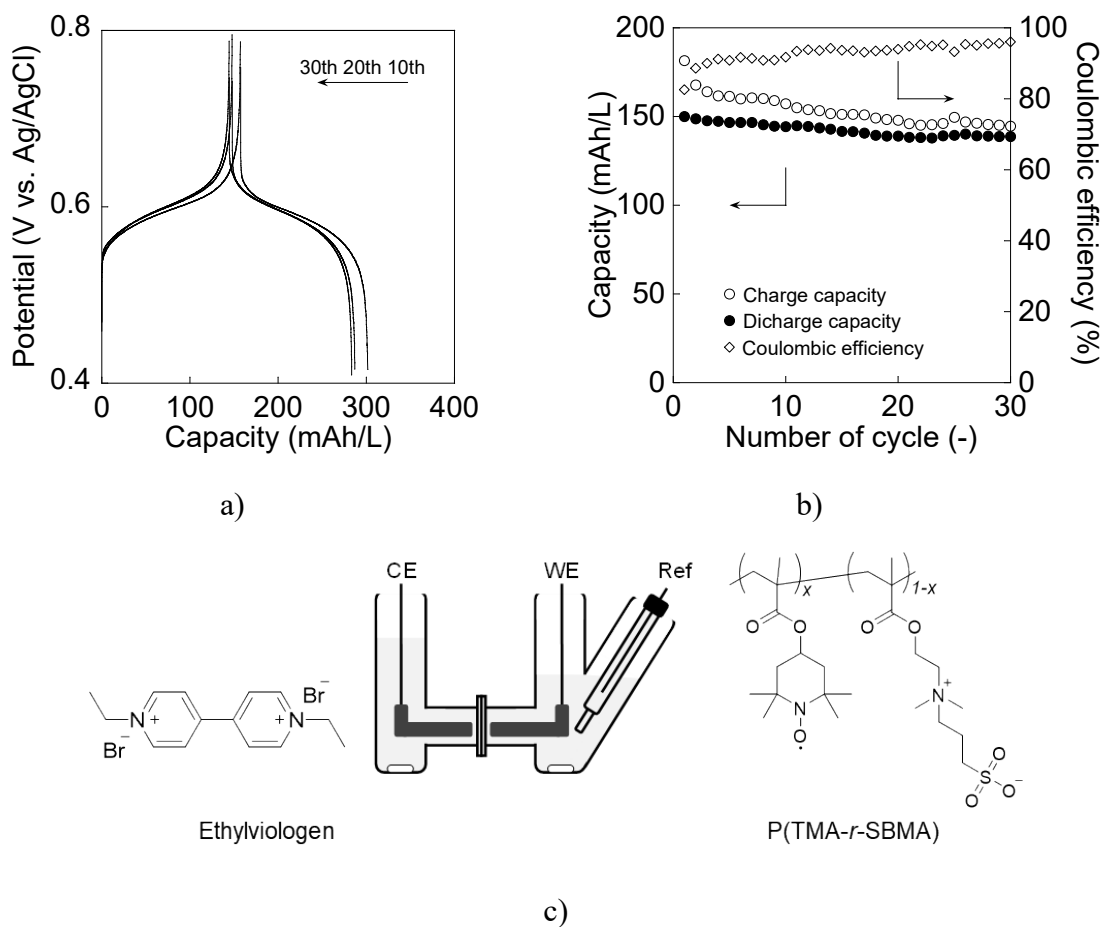
a)

b)

c)

Figure S13. a) 10th, 20th, and 30th charge-discharge curves of the half-cell of P(TMA-*r*-SBMA), measured at 0.5 C. b) Cycle performance. c) Cell configuration. Ethylviologen (300 mAh/L) was dissolved on the counter side.
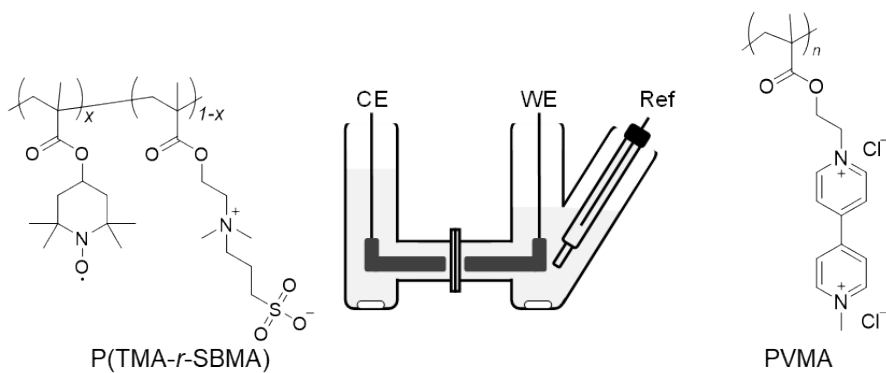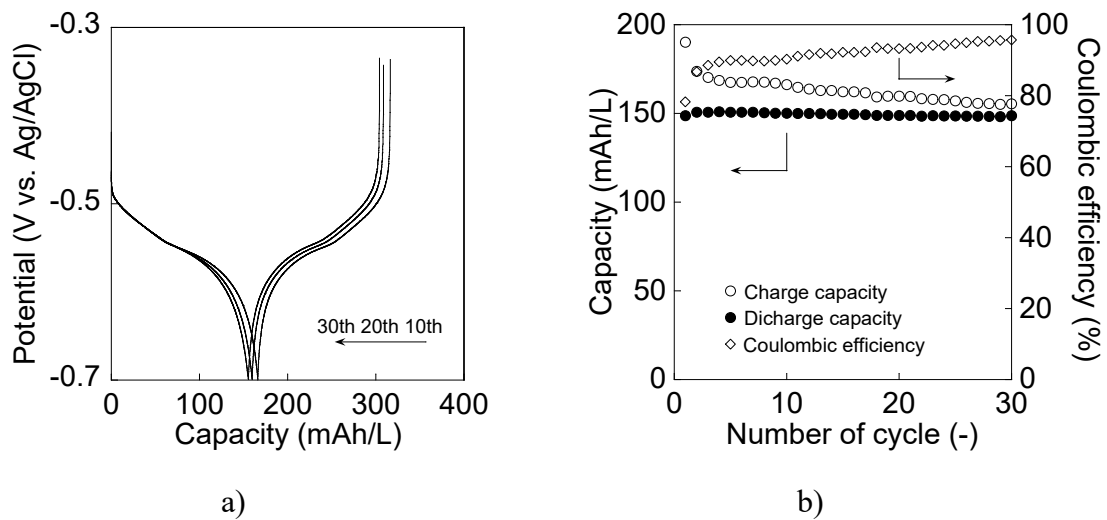
a)

b)

c)

P(TMA-*r*-SBMA)

PVMA

Figure S14. a) 10th, 20th, and 30th charge-discharge curves of the half-cell of PVMA, measured at 0.5 C. b) Cycle performance. c) Configuration of the cell. P(TMA-*r*-SBMA) (300 mAh/L) was dissolved on the counter side.
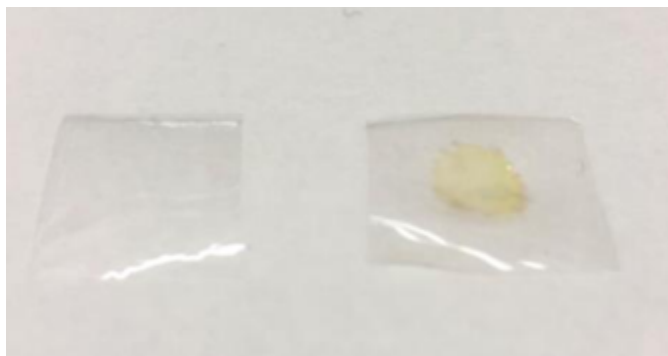
Figure S15. Photograph of a Nafion film as a separator. The left image shows a film before measurement. After repeating charge/discharge cycles, the film is colored yellow because of the absorption of active materials (right image).
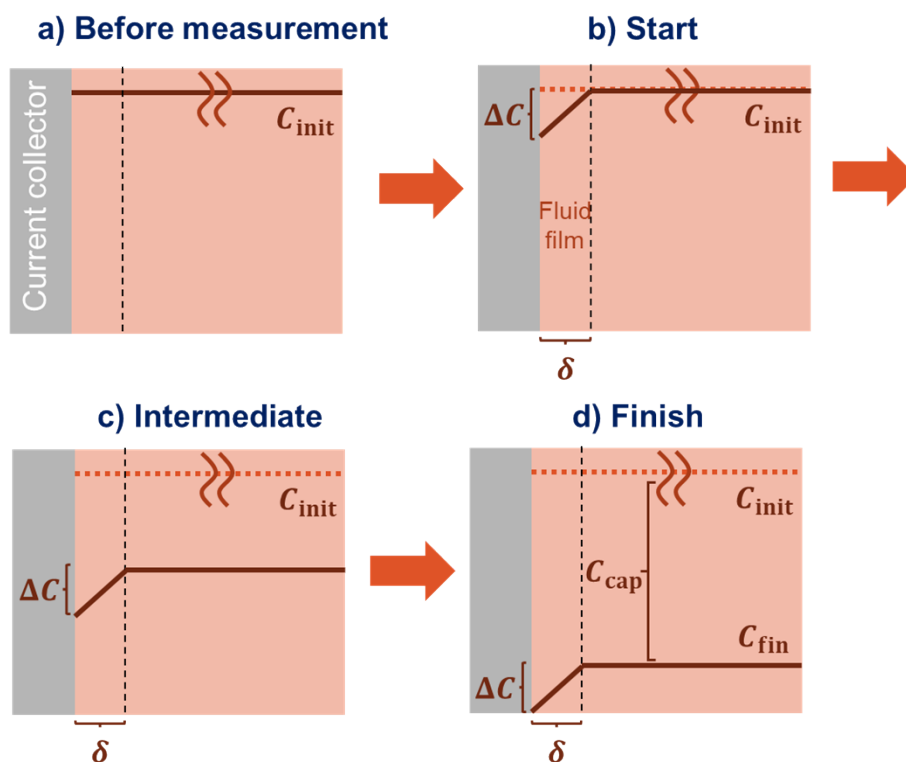
Figure S16. Ideal scheme of chronopotentiometry in liquid-type redox cells.

a) Before measurement, the concentration of active material is constant C_{init}.

b) A fluid film is formed near the current collector just after the beginning of electrolysis. Its thickness δ and concentration change ΔC if fixed because of the constant current measurement. Concentrations in other regions become constant if the system is stirred or flowed sufficiently.

c) During electrolysis, δ and ΔC are constant.

d) The measurement finishes when the concentration of the active material reaches zero at the current collector. The chargeable concentration C_{cap} equals to $C_{init} - C_{fin} = C_{init} - \Delta C$.

References

1. E. C. Montoto, G. Nagarjuna, J. Hui, M. Burgess, N. M. Sekerak, K. Hernandez-Burgos, T. S. Wei, M. Kneer, J. Grolman, K. J. Cheng, J. A. Lewis, J. S. Moore and J. Rodriguez-Lopez, *J. Am. Chem. Soc.*, 2016, **138**, 13230-13237.
2. T. Janoschka, N. Martin, U. Martin, C. Friebe, S. Morgenstern, H. Hiller, M. D. Hager and U. S. Schubert, *Nature*, 2015, **527**, 78-81.
3. Y. Y. Lai, X. Li and Y. Zhu, *ACS Appl. Polym. Mater.*, 2020, **2**, 113-128.
4. K. H. Hendriks, S. G. Robinson, M. N. Braten, C. S. Sevov, B. A. Helms, M. S. Sigman, S. D. Minteer and M. S. Sanford, *ACS Cent. Sci.*, 2018, **4**, 189-196.

5.   K. Hatakeyama-Sato, T. Nagano, S. Noguchi, Y. Sugai, J. Du, H. Nishide and K. Oyaizu, *ACS Appl. Polym. Mater.*, 2019, **1**, 188-196.

6.   R. W. Murray, *Molecular Design of Electrode Surfaces*, Wiley- Interscience, New York, 1992.

7.   K. Sato, R. Ichinoi, R. Mizukami, T. Serikawa, Y. Sasaki, J. Lutkenhaus, H. Nishide and K. Oyaizu, *J. Am. Chem. Soc.*, 2018, **140**, 1049-1056.

8.   C. Clasen, J. P. Plog, W. M. Kulicke, M. Owens, C. Macosko, L. E. Scriven, M. Verani and G. H. McKinley, *J. Rheol.*, 2006, **50**, 849-881.

9.   D. Papanagopoulos, E. Pierri and A. Dondos, *Polymer*, 1998, **39**, 2195-2199.

10.   F. J. Vidal-Iglesias, J. Solla-Gullón, V. Montiel and A. Aldaz, *Electrochem. Commun.*, 2012, **15**, 42-45.

11.   T. Suga, Y. J. Pu, K. Oyaizu and H. Nishide, *Bull. Chem. Soc. Jpn.*, 2004, **77**, 2203-2204.

12.   J. B. Allen and R. F. Larry, *Electrochemical Methods: Fundamentals and Applications, 2nd Edition*, John Wiley & Sons, 2001.

13.   K. Oh, S. Won and H. Ju, *Electrochim. Acta*, 2015, **181**, 13-23.

14.   R. Banerjee, N. Bevilacqua, A. Mohseninia, B. Wiedemann, F. Wilhelm, J. Scholta and R. Zeis, *J. Energy Storage*, 2019, **26**, 100997.